Fermi National Accelerator Facility

INFN-SSSA Summer Internship Final Report

1.3GHz SRF CAVITIES THERMAL TREATMENTS: A PATH TO HIGH Q-FACTORS

Supervisor:

Anna Grassellino

Intern:

Mattia Checchin

Summer 2013

Index

1 Cavities thermal diffusion doping

It was demonstrated [1], that by controlling the impurities concentration at the inner surface, it is possible to modify the superconducting behavior of the cavity, and then its performances.

My project at FNAL was focused on the implementation of a new approach of thermal Nitrogen doping of $1.3 GHz$ single-cell Niobium cavities, in order to maximize the quality factor. In this section it will be shown the furnace used, the state of the art of the technique and the new thermal treatment proposed.

1.1 FNAL classical bake system

The Fermilab's facility consists in a classic UHV furnace. This can provide different types of thermal process till temperatures up to $1000°C$, with the possibility to introduce, with a mass flow controller, precise amounts of gasses inside the chamber. In Fig. 1.1 it is shown the furnace and a nine-cell $1.3 GHz$ cavity ready to be treated.

The heating, with this kind of standard UHV furnaces, is provided by several heating elements that surrounds the load without touch it. In this particular case several 2 inch Molybdenum strips are positioned around the cavity and the heating is performed by irradiation. The heating ramp is therefore longer than for our UHV inductive annealing approach and the temperature varies much more slowly. This furnace is provided of a vacuum pumping system, which is composed of a dry mechanical roughing pump and of a $4800\, l/s$ cryogenic pump. As it can be seen from the Fig. 4.12, the furnace is pretty big, therefore it can accommodate one nine-cell or two single-cell $1.3 GHz$ cavities per process. At FNAL they also study other kinds of frequency and cavity shapes, so the same oven is also used to bake $650 MHz$ single-cells and 350MHz spoke resonators.

The main advantage of this kind of baking system is the high automation. It gives in fact the possibility to program the thermal cycles and the gasses flow, by a computer interface.

1.2 The state of art of cavity doping

The state of art of impurity doping in cavities technology, is based on the diffusion of gaseous species through a thermal treatment in an UHV environment. The typical parameter of such kind of process are $800 - 1000°C$ for 10 minutes in atmosphere of Nitrogen ($2 \cdot 10^{-2} torr$) and a preliminary pressure of $10^{-7} torr$.

Figure 1.1: In figure is shown a $1.3 GHz$ nice-cell cavity ready to be baked inside the furnace.

This situation is simply explained with the Fick laws [2], in the approximation of isotropic media. For simplicity the presence of grain boundaries is not taken into account. The net flux of particles which travel through two points of a concentration gradient is defined from the first Fick law:

$$\boldsymbol{J} = -D\boldsymbol{\nabla}C \tag{1.1}$$

where D is the diffusion coefficient, which is described with an Arrhenius behavior:

$$D = D_0 \cdot e^{-\frac{E}{k_B T}} \tag{1.2}$$

with E the activation energy of the diffusion process.

By defining the continuity equation, to describe the rate of particles accumulation as function of the concentration with time, $\boldsymbol{\nabla} \cdot \boldsymbol{J} = \frac{\partial C}{\partial t}$, the second Fick law is the following:

$$\frac{\partial C}{\partial t} = \boldsymbol{\nabla} \cdot (D\boldsymbol{\nabla}C) \tag{1.3}$$

In the case under study the pressure of the gas during the process is constant, therefore the concentration profile is defined by the "constant source" solution of the second Fick law:

$$C(x) = C_s \cdot \mathrm{erfc}\left(\frac{x}{2\sqrt{Dt}}\right) \tag{1.4}$$

where C_s is the concentration at the surface, which correspond to the solid solubility of the diffused species in the material. During the whole process the concentration at the surface is constant, and it will depend only on temperature and pressure. Some Nitrogen diffusion profiles in Niobium were calculated and are shown in Fig. 1.2, using the diffusion data of Nitrogen in Niobium reported in [3].
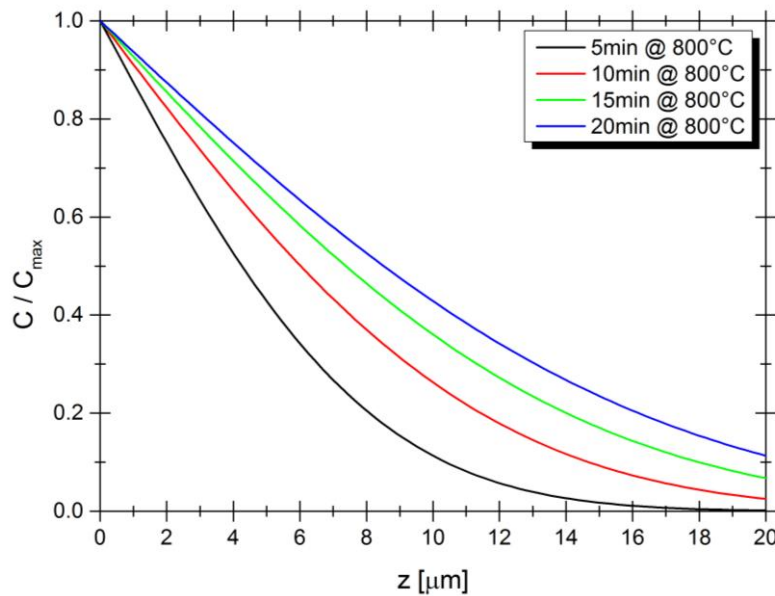
Figure 1.2: Some "constant source" diffusion profiles calculated for Nitrogen in Niobium.

The idea at the basis of this kind of thermal treatment is to improve the superconducting behavior of the cavity during its working. In fact, the BCS surface resistance is strictly dependent on the electrons mean free path and shows a minimum around $20 nm$. With such kind of process the mean free path changes because of the impurities diffused, so in principle it is possible to modify the BCS resistance in order to minimize it.

Because of the London penetration depth in the superconducting state, the surface resistance of the superconductor depends only on the concentration of impurities near the surface. Therefore, in order to reach the wanted surface concentration, it becomes necessary to remove material from the inner surface exposing, step by step, different concentrations. This is done with an electrochemical approach that take advantage of electro-polishing. An example of such thermal

process, done to the cavity TE1AES005, is shown in Fig. 1.3. The parameter where 10 minutes at 800°C in a Nitrogen atmosphere of $2 \cdot 10^{-2} torr$.
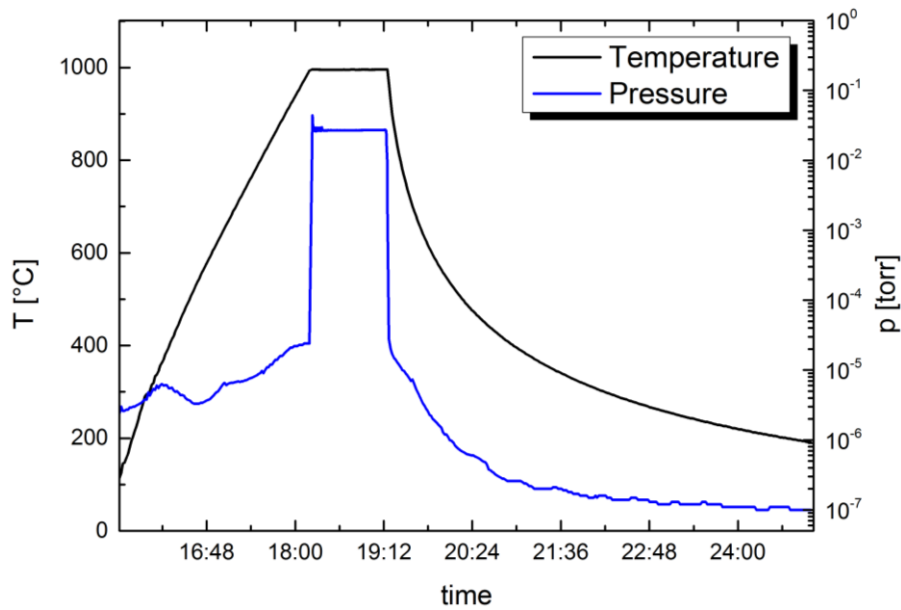
Figure 1.3: Thermal treatment of cavity TE1AES005.
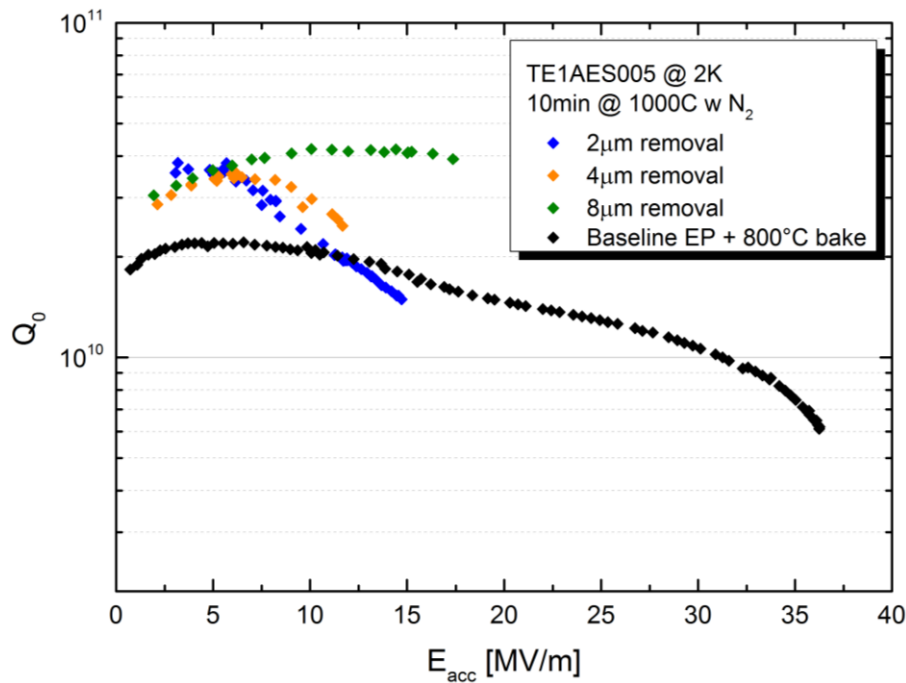
Figure 1.4: Quality factor versus accelerating or the cavity TE1AES005 at the temperature of $2K$ for different amount of material removed, courtesy of A. Grassellino .

The correct amount of material removal from the inner surface is decided by RF testing the cavity. As the material removal increases the cavity behavior changes, therefore when the best result is obtained the correct surface concentration is reached. Indeed, in order to reach the correct

surface concentration to maximize the Q-factor, several material removal steps are needed. An example of this kind of approach is shown in Fig. 1.4. The black points refer to a standard no-doped cavity, while the green, red and blue ones refer to the cavity after the doping treatment and after sequential steps of material removal from the inner surface via electro-polishing. The depths removed were respectively $2\mu m$, $4\mu m$ and $8\mu m$.

It can be noticed in Fig. 1.4, that the shape of the curve changes radically respect the normal behavior (black points), and shows higher Q-factors. The most noticeable fact is that the curves present a maximum, which moves to higher field as the material removal increases. The correct amount of material removed from the inner surface, is then decided by this approach based on RF tests and subsequent chemical processes.

The cons of the process described is the needing of a really accurate chemical process to remove material from the inner surface, therefore to produce cavities always with the same behavior in the mass production, this may become a really critical problem. A possible solution to this issue is to develop a chemistry-free process, in which material removal from the inner surface is not needed. The solution, as it will be explained after, might be found in the "finite source" diffusion solution of the second Fick law.

1.3 The new approach to cavity doping

The new approach proposed is focused on the control of the surface concentration without needing of post chemistry processes. This can be done by dividing the normal diffusion process in two different steps.

The first step is needed to let the diffusing species to be absorbed from the material, the second one is instead thought to let them diffuse without any other source of dopants. This practically means to:

1. Heating the cavity in the furnace for a certain time in the dopant atmosphere. This step is practically the same thermal treatment used till now, described by the constant source diffusion solution with the typical profile shown in Fig. 1.2. Then, the total amount of dopants M will be the area subtended to the concentration profile.

2. After some time, when the total amount of diffused dopants wanted is reached, the pressure of the doping gas inside the furnace is reduced to zero, and maintaining the same temperature, the dopant is left to diffuse till the right surface concentration is reached.

This second step can be simulated by considering the "finite source" solution of the second Fick law:

$$C(x,t) = \frac{M}{\sqrt{\pi Dt}} \cdot e^{-\frac{x^2}{4Dt}} \qquad (1.5)$$

where M is the concentration per unit of area of the dopant. This formulation is valid in the case of an infinitesimal thin layer on the material's surface, which starts to diffuse at the time $t = 0$. The interesting aspect of this equation is that the surface concentration in not anymore constant with time, it in fact varies:

$$C_s(t) = \frac{M}{\sqrt{\pi Dt}} \qquad (1.6)$$

Therefore, in principle, it is possible to reach a certain target surface concentration simply by controlling the temperature and the time of the process. Some diffusion profiles calculated are shown in Fig. 1.5.
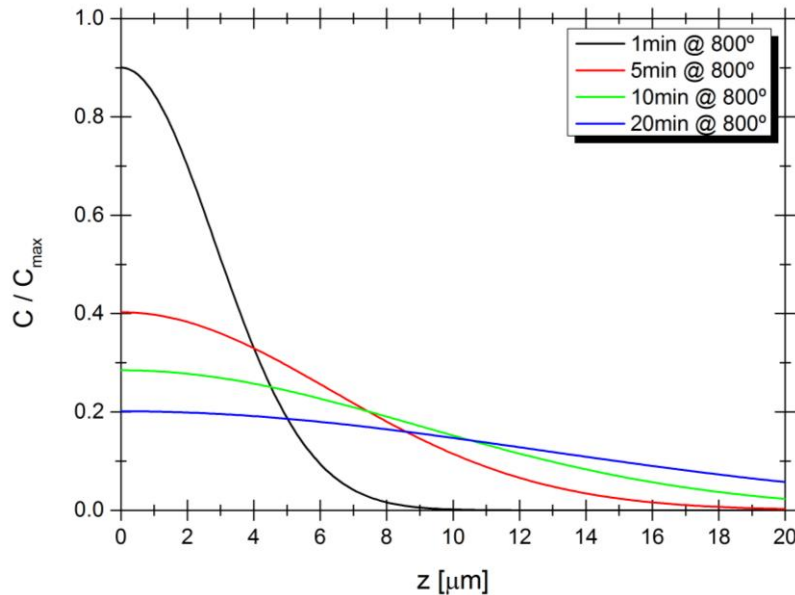
Figure 1.5: Some "finite source" diffusion profiles calculated for Nitrogen in Niobium.

Some problems arise when the profile concentration after the second step is calculated using the number of dopants per unit of area M defined in the first step. This because, as discussed earlier, the "finite source" solution is formulated in the approximation of an infinitesimal thin layer of dopants at the surface, while in the case of the first step a diffusion profile is obtained. This means that the dopants profile distribution after the second step is only a roughly simulation of how really the concentration gradient after the thermal treatment appears.

By the way to maintain consistency between first and second step, the total mass of dopants conservation is mandatory. This means that the total number of species diffused in the first step has to be conserved during the second one. To do that let us consider the total amount of atoms per unit of area M, which correspond to the area subtended the diffusion profile of the first step:

$$M = \int_0^\infty C_s \cdot \text{erfc}\left(\frac{x}{2\sqrt{Dt}}\right) dx \qquad (1.7)$$

The concentration profiles were calculated in order to reach a certain target surface impurities relative concentration. In fact, the real concentration at the surface after the first step was unknown. The target relative concentration chosen was the surface concentration of a normal thermal doping process (10 minutes at $800°C$ in atmosphere of $2 \cdot 10^{-2} torr$ of Nitrogen) after $8\mu m$ of material removal.

In Fig. 1.6 it is shown the doping profile after such process. The black arrow indicates the target surface relative concentration after $8\mu m$ of material removal ($C_s/C_{max} = 0.37$). This concentration was chosen because the cavity treated in such way showed a good behavior.
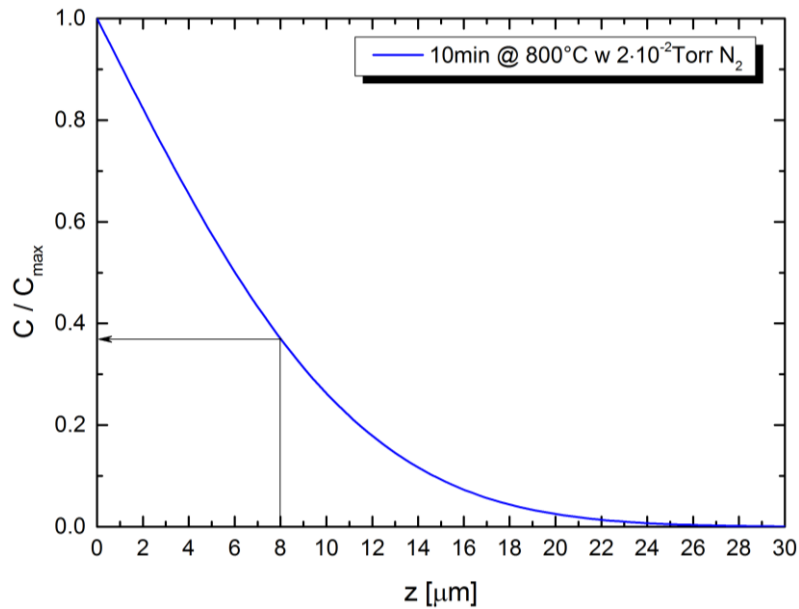
Figure 1.6: 10 minutes at $800°C$ in atmosphere of $2 \cdot 10^{-2} torr$ of Nitrogen thermal profile.

In order to simplify the process the temperature of the first and second step was maintained constant, therefore the only parameter that can be optimize in order to modify the surface concentration, for a fixed M, is the duration of the second step t. So, in order to obtain a certain target surface concentration C_s, the process duration will be:

$$t = \left(\frac{1}{\pi D}\right)\left(\frac{M}{C_s}\right)^2 \tag{1.8}$$

Two different thermal processes were implemented to two different $1.3 GHz$ single-cell elliptical cavities. The first process was thought to be at higher temperature $800°C$, the second oe at lower temperature $300°C$.

In the following table (Tab. 1.1) are shown the two thermal treatments implemented:

Cavity #	1st step	2nd step
TE1AES011	2' @ 800°C + 2·10^{-2}torr of N$_2$	6' @ 800°C
TE1ACC001	4h @ 300°C + 2·10^{-2}torr of N$_2$	12h30' @ 300°C

Table 1.1: Thermal doping treatments done at FNAL.

The two diffusion profiles calculations, for the first and second step, are shown in Fig. 1.7, with the respective temperature and pressure profiles during the process.

As it can be seen from the two thermal profiles in Fig. 1.7b and 1.7d, the doping process is preceded by a standard process at $800°C$ for 3 hours, which aim is to degas impurity such as Hydrogen. This kind of process is the typical $800°C$ bake performed for every cavity currently used inside accelerators.

Such kind of $800°C$ thermal treatment performed at FNAL is slightly different from other laboratories. In fact it was found that the FNAL's furnace is contaminated by Titanium, which during such kind of process ends up to contaminate the cavity surface [4]. Therefore the $800°C$ bake is always performed with the cavity cut-offs closed with a cap. The cap is projected to let the desorbed gasses to come out from the cavity through some lateral holes, but to block all the line-of-sight trajectories of Titanium atoms from the furnace environment.

Only the cavity TE1ACC001 takes advantage of these caps, the cavity TE1AES011 does not. This last was then electro-polished to eliminate $2\mu m$ of Titanium-contaminated material from the inner surface, hence the concentration at the surface was different respect the one previously calculated.

By the way, these two thermal treatments are completely different and determine two completely different diffusion profiles. The high temperature one gives a profile with a depth of tens of microns, while the low temperature one only of $100nm$. This choice was done in order to

study how the superconductive properties of the cavity are affected from different gradients of dopants, i.e. mean free path.
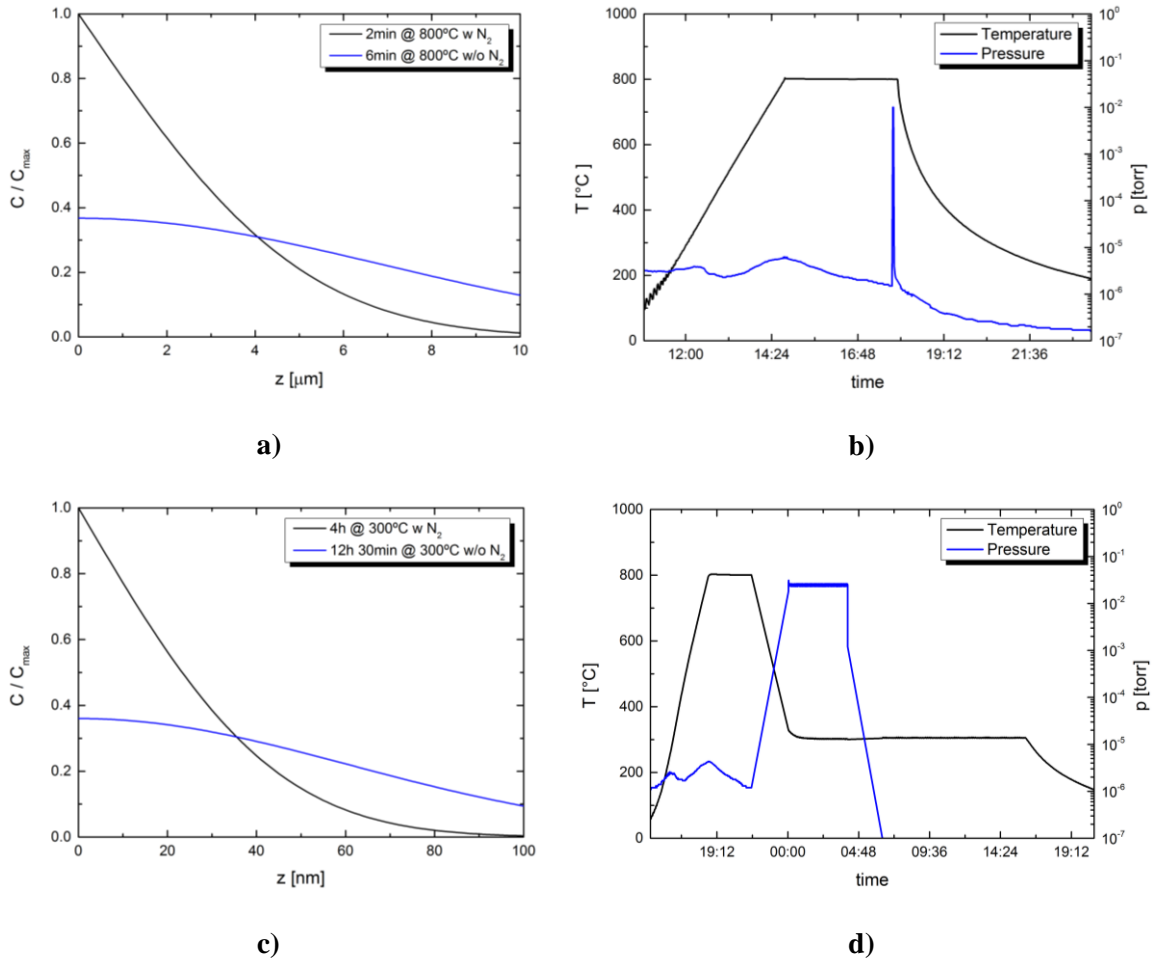
Figure 1.7: High temperature thermal doping on cavity TE1AES011. In figure a) is shown the simulation of the diffusion profile, while in figure b) is shown the thermal and pressure profile during the process. Low temperature thermal doping on cavity TE1ACC001. In figure c) is shown the simulation of the diffusion profile, while in figure d) is shown the thermal and pressure profile during the process.

In fact, the London penetration depth, within the electromagnetic wave can oscillate at the surface of the superconductor, for very clean and electro-polished Niobium is about $23 nm$ [5] instead in the dirty limit it can reach $50 nm$. Hence, in the high temperature process the impurities concentration is approximate constant inside the London penetration depth, in the low temperature ones, instead, the opposite situation happens and the impurity concentration is not constant. We then expect that the BCS surface resistance will be affected differently in the two cases.

2 The BCS Surface Resistance

In order to calculate the superconducting surface resistance S. B. Nam in the 1956 defines that by considering a complex conductivity $\sigma_1 - i\sigma_2$ the formulation of the normal conducting skin effect [6] can be extended to the superconducting case [7, 8]:

$$\frac{R_s(\omega) + iX_s(\omega)}{R_n(\omega) + iX_n(\omega)} \approx \left(\frac{\sigma_1(\omega) - i\sigma_2(\omega)}{\sigma_n(\omega)}\right)^m \tag{2.1}$$

where the exponent m varies between:

- $m = -\frac{1}{2}$ $\rightarrow$ London's limit

- $m = -\frac{1}{3}$ $\rightarrow$ Pippard's limit

The surface resistance $R_s(\omega)$ and reactance $X_s(\omega)$ can be rewritten as:

$$\frac{R_s}{R_n} = \mathcal{R}e\left\{\frac{\sigma_1}{\sigma_n} - i\frac{\sigma_2}{\sigma_n}\right\}^m - \frac{X_n}{R_n}\mathcal{I}m\left\{\frac{\sigma_1}{\sigma_n} - i\frac{\sigma_2}{\sigma_n}\right\}^m$$

$$\tag{2.2}$$

$$\frac{X_s}{X_n} = \mathcal{R}e\left\{\frac{\sigma_1}{\sigma_n} - i\frac{\sigma_2}{\sigma_n}\right\}^m + \frac{R_n}{X_n}\mathcal{I}m\left\{\frac{\sigma_1}{\sigma_n} - i\frac{\sigma_2}{\sigma_n}\right\}^m$$

By considering only the resistance part of the superconductor response to the external electromagnetic field and in the assumption of London limit ($m = -1/2$), R_s/R_n can be rewritten as:

$$\frac{R_s}{R_n} = \frac{1}{\sqrt{2}}\frac{\left\{\left[\left(\frac{\sigma_1}{\sigma_n}\right)^2 + \left(\frac{\sigma_2}{\sigma_n}\right)^2\right]^{1/2} - \left(\frac{\sigma_2}{\sigma_n}\right)\right\}^{1/2}}{\left[\left(\frac{\sigma_1}{\sigma_n}\right)^2 + \left(\frac{\sigma_2}{\sigma_n}\right)^2\right]^{1/2}} \tag{2.3}$$

in the approximation that the real part of the complex conductibility is lower than the imaginary part ($\sigma_1 \ll \sigma_2$) and considering the temperature range $T < T_c/2$, which is suitable in the Niobium immersed in liquid Helium case ($4.2K < 9.27K/2$), Eq. 2.3 becomes much simpler:

$$\frac{R_s}{R_n} = \frac{1}{\sqrt{2}}\frac{\frac{\sigma_1}{\sigma_n}}{\left(\frac{\sigma_2}{\sigma_n}\right)^{3/2}} \tag{2.4}$$

as it was defined in the D. C. Mattis and J. Bardeen's work [9], the relationship Eq. 2.1 should be used to calculate the surface impedance of superconductors. But in the approximation of London limit Eq. 2.4 can also be used. Through a time dependent perturbative quantomechanical approach D. C. Mattis and J. Bardeen give the expression for $\frac{\sigma_1}{\sigma_n}$ and $\frac{\sigma_2}{\sigma_n}$ as follows [9]:

$$
\begin{aligned}
\frac{\sigma_1}{\sigma_n} = &\frac{2}{\hbar\omega}\int_{\Delta}^{\infty}[f(E) - f(E + \hbar\omega)]g^+(E)dE \\
&+ \frac{1}{\hbar\omega}\int_{\Delta-\hbar\omega}^{-\Delta}[1 - 2f(E + \hbar\omega)]g^+(E)dE
\end{aligned}
\tag{2.5}
$$

$$
\frac{\sigma_2}{\sigma_n} = \frac{1}{\hbar\omega}\int_{\Delta-\hbar\omega;-\Delta}^{\Delta}[1 - 2f(E + \hbar\omega)]g^-(E)dE
\tag{2.6}
$$

Where $f(E)$ is the Fermi-Dirac distribution, which defines the state occupation at the energy E. The term $f(E + \hbar\omega)$ defines the occupation at the energy $E + \hbar\omega$, where $\hbar\omega$ corresponds to the energy provided to the system from the electromagnetic field. While the value $g^\pm(E)$ is an energetic weight gave to the occupational distributions:

$$
g^\pm(E) = \frac{E^2 + \Delta^2 + \hbar\omega E}{[\pm(E^2 - \Delta^2)]^{1/2}[(E + \hbar\omega)^2 - \Delta^2]^{1/2}}
\tag{2.7}
$$

and the energy gap $\Delta(T)$ is defined as $\Delta(T) = \Delta(0)\sqrt{\cos\left[\frac{\pi}{2}\left(\frac{T}{T_c}\right)^2\right]}$.

The first integral in Eq. 2.5 therefore defines the total number of quasi particles that fall in energy states above the gap that were not been exited by the external perturbation, but only by thermal excitation. In the two fluid model point of view, this integral defines the normal conductive fluid which exists only for $T > 0K$, while at $T = 0K$ all electrons are condensed in Cooper pairs. The second integral defines the number of Cooper pairs broken because of the electromagnetic field. This one does not give a big contribution, so generally it is neglected unless the excitation is bigger than the gap, i.e. $\hbar\omega \geq 2\Delta$. Eq. 2.6 instead considers the imaginary part contribution to the conductivity due to the superelectrons inductive behavior.

The D. C. Mattis and J. Bardeen definitions of real and imaginary parts of the conductivity can be analytically resolved in the normal skin effect regime $\hbar\omega < 2\Delta$ [10].

$$
\frac{\sigma_1}{\sigma_n} = \frac{2\Delta}{k_B T\left(1 + e^{-\Delta/k_B T}\right)^2}\ln\left(\frac{\Delta}{\hbar\omega}\right)e^{-\Delta/k_B T}
\tag{2.8}
$$

$$
\frac{\sigma_2}{\sigma_n} = \frac{\pi\Delta}{\hbar\omega}\tanh\left(\frac{\Delta}{2k_B T}\right)
\tag{2.9}
$$

In Fig. 2.1 it is shown the shape of the two contributions on the complex conductivity of a superconductor respect to the temperature.
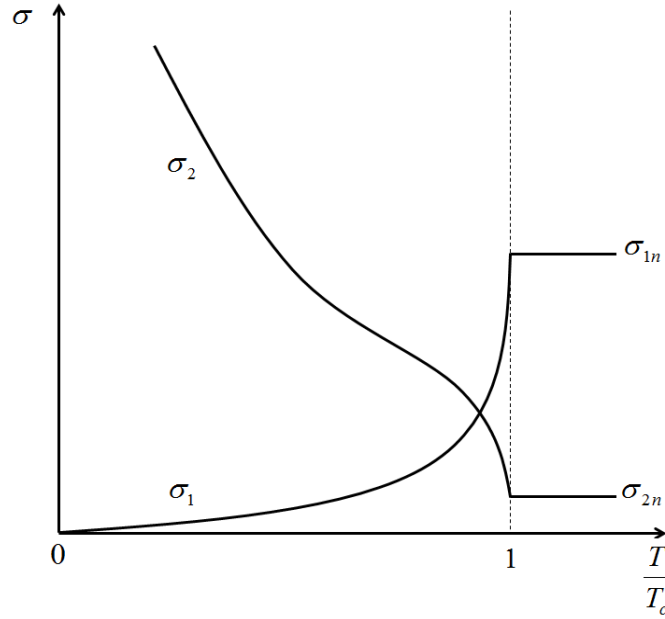
Figure 2.1: Real and imaginary parts of conductivity for a superconductor.

As the temperature decreases the real part contribution gets smaller, because of the number of quasi-particle over the gap drops as the temperature decreases ($\hbar\omega < 2\Delta$ so we only consider thermally excited quasi-particles). Vice versa, the imaginary part becomes bigger as the temperature decreases, indeed as the superelectrons grow in number, the inductive behavior of the superconductor becomes bigger.

By direct substitution of Eq. 2.8 and 2.9 in the Nam derivation of superconductive skin effect (Eq. 2.4), in the approximation of $\sigma_1 \ll \sigma_2$ and $T < T_c/2$, one obtain:

$$R_{BCS} = \frac{R_n}{\sqrt{2}} \frac{2\Delta}{k_B T} \left(\frac{\hbar\omega}{\pi\Delta}\right)^{\frac{3}{2}} \ln\left(\frac{\Delta}{\hbar\omega}\right) \frac{e^{-\Delta/k_B T}}{\tanh^{\frac{3}{2}}\left(\frac{\Delta}{2k_B T}\right)\left(1 + e^{-\Delta/k_B T}\right)^2} \tag{2.10}$$

where R_n is the normal conducting resistance:

$$R_n = \sqrt{\frac{\omega\mu_0}{2\sigma_n}} = \sqrt{\frac{\omega\mu_0\rho_n}{2}} \tag{2.11}$$

so the BCS surface resistance becomes:

$$R_{BCS}(\omega, T) = \frac{\sqrt{\omega \mu_0 \rho_n}}{2} \frac{2\Delta}{k_B T} \left(\frac{\hbar\omega}{\pi\Delta}\right)^{\frac{3}{2}} \ln\left(\frac{\Delta}{\hbar\omega}\right) \frac{e^{-\Delta/k_B T}}{\tanh^{\frac{3}{2}}\left(\frac{\Delta}{2k_B T}\right)\left(1 + e^{-\Delta/k_B T}\right)^2}$$

$$= A\sqrt{\rho_n} \frac{e^{-\Delta/k_B T_c}}{\sqrt{sT_c}T\left(1 + e^{-\Delta/k_B T_c}\right)^2} \omega^2 \ln\left(\frac{\Delta}{\hbar\omega}\right)$$

(2.12)

Where $s = 3.56 \div 4$ (for Niobium) is the strong coupling factor, while $A = 6 \cdot 10^{-21}\sqrt{\Omega \cdot K^3/(m \cdot s^4)}$ and ρ_n is the normal conducting resistivity just before the superconductive transition.

Generally this formula is used in a more approximate formulation, which becomes useful during the experimental data fit:

$$R_{BCS}(\omega, T) = \frac{A \cdot \omega^2}{T} \cdot e^{-\Delta/k_B T}$$

(2.13)

Where A is leave as a free parameter with the superconducting energy gap Δ.

From this formulation of the BCS surface resistance, one can notice that as the temperature decreases, also the surface resistance decreases. Indeed the most important dependence of R_{BCS} is on the Arrhenius exponential $e^{-\Delta/k_B T}$, which for $T < T_c/2$ can be expressed as:

$$e^{-\frac{\Delta}{k_B T}} = e^{-\frac{sT_c}{2T}} \qquad ; \qquad \Delta(T) \cong \Delta_0 = \frac{s}{2}k_B T_c$$

(2.14)

in this way it was highlighted the fact that superconductors with higher transition temperature have lower surface resistance, but also the normal conducting resistivity plays an important role, in fact as it is shown in Eq. 2.12 R_{BCS} decreases as ρ_n decreases.

2.1 The Residual Resistance

As always the theoretical previsions are not completely correct. Indeed, the surface resistance of a superconductor is not only due to the BCS contribution, but generally for measurements at $T < 0.2T_c$ it happens that the surface resistance reaches a constant value called residual surface resistance R_{res}. We should then express the surface resistance of a semiconductor as two contribution, one temperature dependent, R_{BCS}, and one not, as it is shown in Fig. 2.2.

The global surface resistance of the superconductor, R_s, is therefore defined as:

$$R_s = R_{BCS}(T) + R_{res} \tag{2.15}$$

Generally, this constant residual contribution for Niobium cavities is of the order of $5 - 10n\Omega$. Several effects affect the residual resistance, some examples are [11]:

- DC fluxoids dissipation

- Niobium Hydrides Q-disease

- Impurities segregation at grains boundaries

Practically all kind of dissipation mechanisms that do not belongs to the BCS contribution becomes part of the residual resistance.
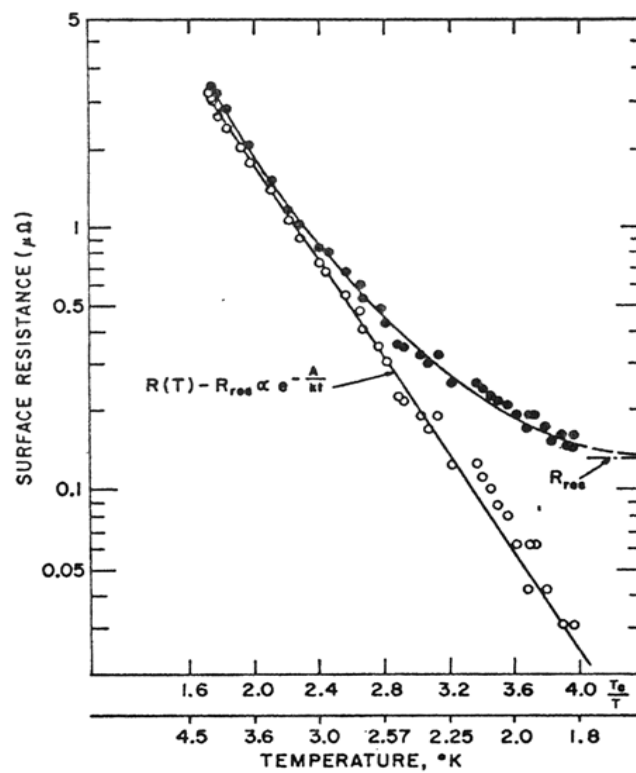
Figure 2.2: Surface resistance of a superconductor as function of the temperature.

3 The BCS Surface Resistance Dependence on Mean Free Path

As it was shown the first time from A. B. Pippard [12], the impurities content inside the superconductor modifies radically the superconductor response to an external perturbation, such as an electromagnetic field. Pippard shown that if the normal electrons mean free path changes, then the coherence length also changes, implying that the description of the material response in term of current density varies from a local description (dirty limit) to a non-local one (clean limit).

This dependence of the persistent currents in the DC case, is anyhow really interesting in our case, in fact, also in the AC case the impurities content modifies the system response.

Let us return to consider Eq. 2.8. From the London formulation of penetration depth ($\lambda_L = \sqrt{\frac{m}{\mu_0 n_s e^2}} = \sqrt{\frac{1}{\omega \mu_0 \sigma_s}}$), where $\sigma_s \equiv \sigma_2$ one can obtain:

$$\frac{\sigma_2}{\sigma_n} = \frac{\rho_n}{\omega \mu_0 \lambda^2} = \frac{\pi \Delta}{\hbar \omega} \tanh\left(\frac{\Delta}{2 k_B T}\right)$$

(3.1)

$$\Rightarrow \quad \lambda^2 = \frac{\rho_n}{\omega \mu_0} \left(\frac{\pi \Delta}{\hbar \omega} \tanh\left(\frac{\Delta}{2 k_B T}\right)\right)^{-1}$$

Eq. 3.38 we used was calculated in the London limit (extreme dirty limit), for which $l \ll \xi_0$, so Eq. 3.16 becomes:

$$\lambda \cong \lambda_L \left(\frac{\xi_0}{l}\right)^{1/2}$$

(3.2)

therefore, by equaling Eq. 3.1 and Eq. 3.2 one obtain:

$$\lambda_L{}^2 \frac{\xi_0}{l} \cong \frac{\rho_n}{\omega \mu_0} \left(\frac{\pi \Delta}{\hbar \omega} \tanh\left(\frac{\Delta}{2 k_B T}\right)\right)^{-1}$$

(3.3)

In order to extend the R_{BCS} treatment done till here, we can assume to not commit a big error if we use Eq. 3.3 inside the Pippard definition of penetration depth $\lambda_{eff} = \lambda_L \left(1 + \frac{\xi_0}{l}\right)^{\frac{1}{2}}$, which becomes:

$$\lambda^2 = {\lambda_L}^2 + \frac{\rho_n}{\omega\mu_0}\left(\frac{\pi\Delta}{\hbar\omega}\tanh\left(\frac{\Delta}{2k_B T}\right)\right)^{-1} \tag{3.4}$$

It is now possible to calculate the variation of the BCS surface resistance with the mean free path. By considering Eq. 2.4, 2.8 and 2.9, and knowing that Eq. 2.9 may be written as the first formulation of Eq. 3.1, it is possible to rewrite the BCS surface resistance as:

$$R_{BCS} = \frac{R_n}{\sqrt{2}}\left(\frac{\sigma_1}{\sigma_n}\right)\left(\frac{\omega\mu_0\lambda^2}{\rho_n}\right)^{\frac{3}{2}} \tag{3.5}$$

By introducing Eq. 2.11 and our extension to the clean limit with Eq. 3.4, in the R_{BCS} formula, it becomes:

$$R_{BCS} = \frac{1}{2}\left(\frac{\sigma_1}{\sigma_n}\right)(\omega\mu_0\rho_n)^{\frac{1}{2}}\left(\frac{\omega\mu_0}{\rho_n}\lambda_L^2 + \frac{1}{\frac{\sigma_2}{\sigma_n}}\right)^{\frac{3}{2}} \tag{3.6}$$

In order to highlight the dependence on the electrons mean free path, it is necessary to think about how the resistivity ρ_n of normal conducting electrons behave with temperature. By cooling a metal with cryogenic fluids what we see is that the resistivity decreases with the temperature, till it reaches a steady value called residual resistivity.

We can imagine that the resistivity is composed of two different contributions (as shown in Fig. 3.1), one temperature dependent, which is due to the electrons-phonons scattering ($\rho_{ph}(T)$), and another not dependent on temperature, but only on static scattering centers density as impurities, grain boundaries, dislocations and so on (ρ_{res}).

$$\rho_n(T) = \rho_{ph}(T) + \rho_{res} \tag{3.7}$$

It is therefore possible to define a useful parameter called Residual Resistivity Ratio, RRR, as the ratio between the global resistivity temperature dependent at $300K$, over the residual resistance:

$$RRR = \frac{\rho_n(300K)}{\rho_{res}} = 1 + \frac{\rho_{ph}(300K)}{\rho_{res}} \tag{3.8}$$

This parameter it is very important because gives an idea of the purity of the material. As the triple R increases also the purity increases (ρ_{res} increases).

At the temperature of exercise of superconducting cavities, the DC resistivity of Niobium is of course tending to zero because of the superconductive transition. But in the normal state, just above the transition temperature, the resistivity is already the residual one.

This means that in the formula Eq. 3.6, the normal conducting resistivity ρ_n coincides with the residual resistivity ρ_{res}, so we can write:

$$\rho_n \equiv \rho_{res} = \frac{\rho_{ph}(300K)}{RRR - 1} \tag{3.9}$$

As it was just said, the Residual Resistivity Ratio estimates the material purity, hence it is directly related to the electrons mean free path. The formula that relates the two quantities is the following [10]:

$$l = \alpha \cdot (RRR - 1) \tag{3.10}$$

where:

$$\alpha = \frac{\omega \mu_0 \xi_0 \lambda_L^2}{\rho_{ph}(300K)} \frac{\sigma_2}{\sigma_n} \tag{3.11}$$

We have now all the dependencies to express the BCS surface resistance as function of the mean free path. Eq. 3.6 becomes:

$$R_{BCS} = \frac{1}{2} \left(\frac{\sigma_1}{\sigma_n} \right) \left(\frac{\omega \mu_0 \alpha \rho_{ph}(300K)}{l} \right)^{\frac{1}{2}} \left(\frac{\omega \mu_0 \lambda_L^2}{\alpha \rho_{ph}(300K)} l + \frac{1}{\frac{\sigma_2}{\sigma_n}} \right)^{\frac{3}{2}} \tag{3.12}$$
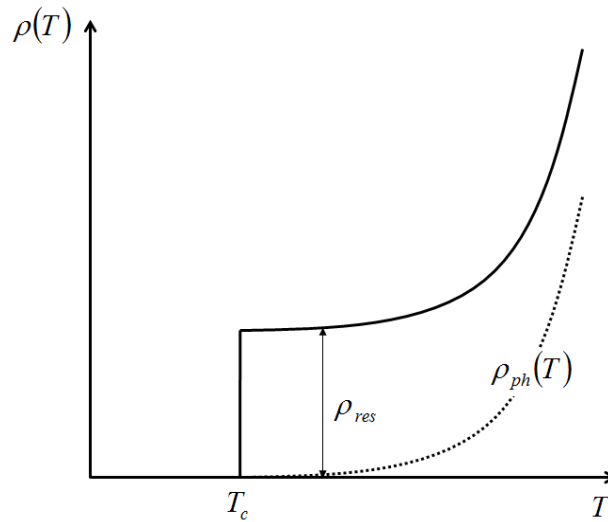
Figure 3.1: The temperature dependence of the normal metals resistivity. If no residual resistivity is present then the resistivity should go to zero at $T = 0K$.
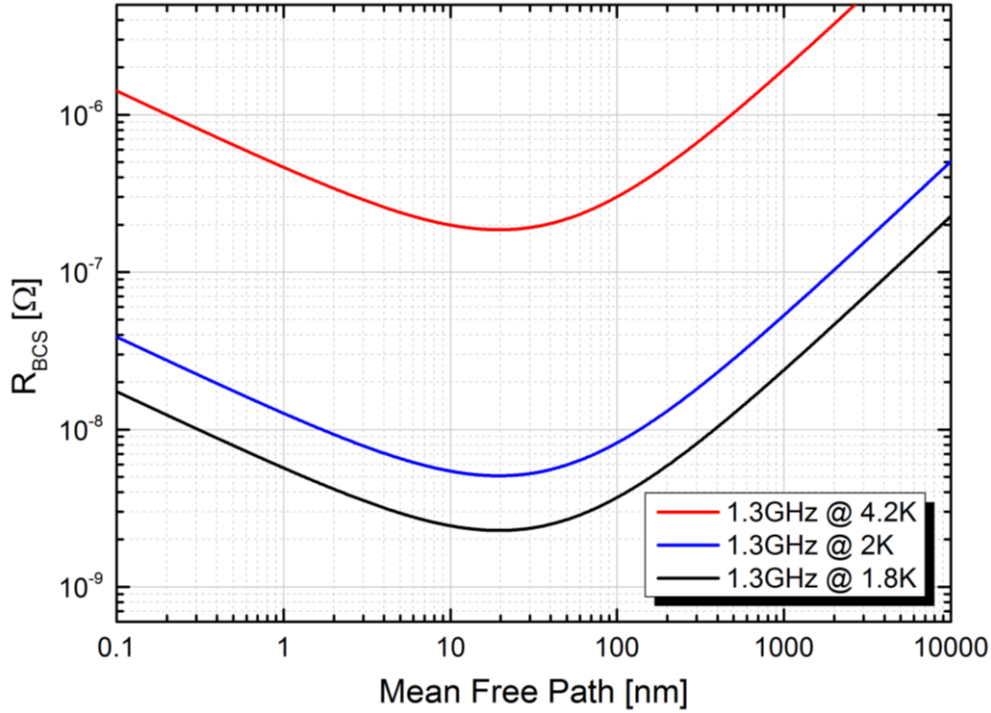
Figure 3.2: Simulation of the BCS surface resistance versus the mean free path for three different temperatures for a frequency of $1.3 GHz$.

However, comparing this results with the R_{BCS} values obtained with more rigorous methods, by considering the specular and diffusive scattering from the surface in the clean limit [11, 13], comes out that in this derivation R_{BCS} is overestimated. But anyhow by multiplying Eq. 3.12 by a constant ($c \cong 1/2$), the results becomes similar.

The interesting features of this equation are the two different dependencies on the mean free path which becomes important in two different regimes.

In the dirty regime $l \ll \xi$, the surface resistance decreases with $l^{-1/2}$, this means that the superconductor behaves as a normal conductive metal which becomes less resistive as the purity increases. But when the mean free path becomes larger than the coherence length, R_{BCS} starts to show an anomalous behavior for which the surface resistance grows with the purity.

From more rigorous derivations [11], it comes out that in the clean limit, $l \gg \lambda, \xi$ the electrons are scattered only from the surfaces of the material, and this means that the BCS resistance becomes independent of the impurity scattering, i.e. of the mean free path.

In Fig. 3.2 it is shown the simulation of the BCS surface resistance for Niobium as function of the mean free path, calculated by using Eq. 3.12 corrected by the factor $1/2$ and the following parameters:

Coherence length, ξ_0	$40 \cdot 10^{-9} m$
London's penetration depth, λ_L	$23 \cdot 10^{-9} m$
Critical temperature, T_c	$9.23 K$
Phonon resistivity at $300K$, $\rho_{ph}(300K)$	$1.45 \cdot 10^{-7} \Omega \cdot m$

As it was expected, the BCS surface resistance shows a minimum around $20nm$. This means that by introducing some impurities, minimizing the mean free path to the correct value, it is possible to reach lower surface resistances and so higher quality factors.

4 Doping studies on $1.3GHz$ cavities

In this section it is presented the work done at FNAL, during my summer internship project on thermal doping of $1.3GHz$ single-cell cavities.

As it was explained in Section 1, a new thermal treatment to dope cavities based on "finite source" diffusion was proposed. Two cavities were prepared with two different processes in order to obtain two completely different concentration profiles. The RF data obtained are then compared with other cavities prepared with the standard doping method, and an explanation of the low field Q-slope is suggested by a model implementation.

Fig. 4.1 shows the results obtained for the "high temperature" treated cavity (TE1AES011) and the "low temperature" treated one (TE1ACC001). To compare the new approach of thermal doping to the standard one, also the cavities TE1AES005 and TE1AES013 were plotted in the same graph. The thermal treatments summary of the cavities studied is shown in Tab. 4.1.

The first thing to notice is the difference between the high temperature treated cavity TE1AES011 and the low temperature one TE1ACC001. The first one shows a very high Q-factor at $2K$, higher than the Q-factors generally obtained with the standard doping method.

Cavity #	Thermal treatment $(p_{N_2} = 2 \cdot 10^{-2} torr)$
Baseline	3h @ 800°C
TE1AES005	10' @ 1000°C w N$_2$ + 8μm removal
TE1AES013	10' @ 800°C w N$_2$ + 7μm removal
TE1AES011	2' @ 800°C w N$_2$ + 6' @ 800°C + 2μm removal
TE1ACC001	4h @ 300°C w N$_2$ + 12h30' @ 300°C

Table 4.1: Cavities treated with the new thermal doping method and standard one.

A really extended low field Q-slope is obtained, with a maximum around $15\,MV/m$. By the way, it is necessary to underline the fact that, this cavity was measured with a fixed coupler in condition of over coupling, therefore a systematic error might be introduced on the measurements, which might imply a translation of the curve and the overestimation of the cavity Q-factor.
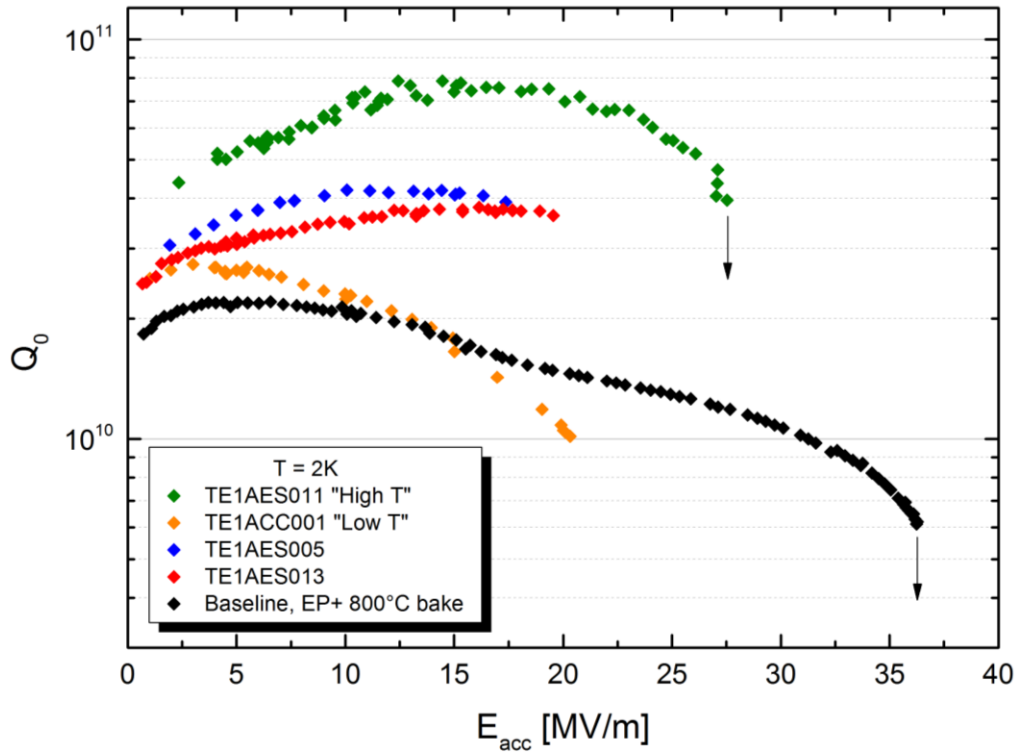
Figure 4.1: In the graph are shown the two cavities treated with the new doping approach, and two cavities treated with the standard approach and the "baseline" cavity after EP and 800°C bake.

The other cavity treated at lower temperatures has instead a completely different behavior: the low field Q-slope is present anyhow, but its elongation is really limited. The main feature of this cavity is instead the pronounced negative Q-slope at medium field.

This observation may suggest an important fact. If the cavity TE1AES011 shows a longer low field Q-slope than cavity TE1ACC001, this means that, the concentration profile of dopants plays a key role. In fact for TE1AES011, as it is shown in Fig. 1.7, the concentration profile is more flat and pretty much constant for about $4\mu m$. On the other hand, TE1ACC001 was treated at lower temperatures, and the concentration profile is pretty much constant only over $40nm$. A possible explanation of the concentration profile effect on the Q-factor dependence on the field will be proposed in next section.

Another important data is the maximum accelerating field. Indeed, the cavity TE1AES011 shows a really high maximum accelerating field too, respect to other doped cavities. The first conclusion we can make is that, the thermal treatment proposed for the cavity TE1AES011 worked not only on the Q-factor value, but also on the maximum accelerating field, by increasing them both. A summary of the cavities studied behavior is reported in Fig. 4.2.
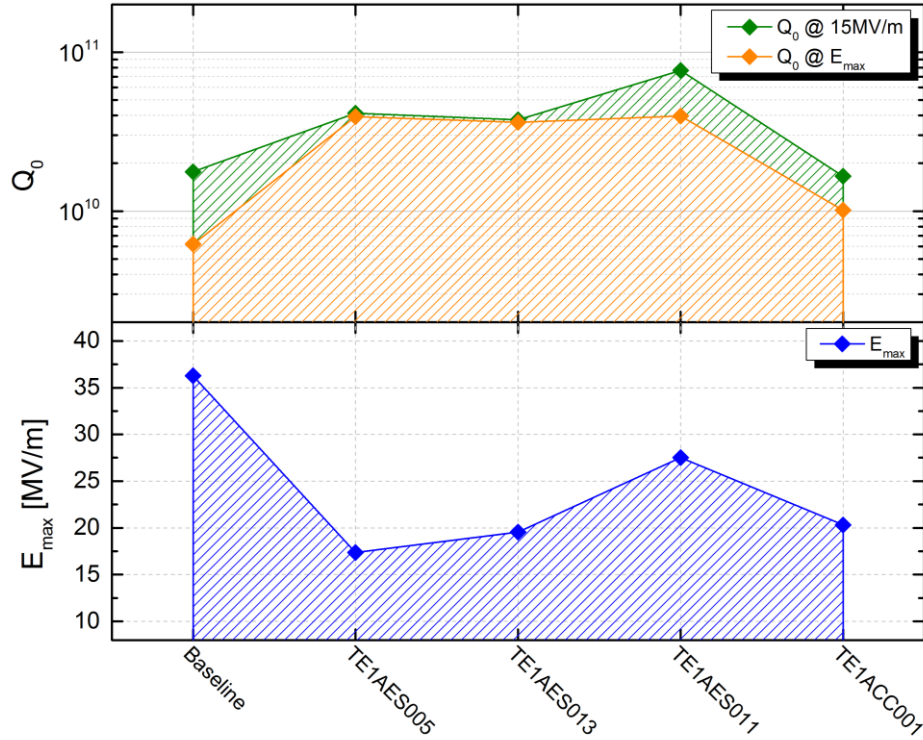
Figure 4.2: Summary of the doped cavities performances.

As it can be seen in Fig. 4.2, generally the doping treatment permits to obtain higher Q-factors, but on the other hand lower accelerating gradients, than standard cavities baked at $800°C$ (in Fig. 4.1 and 4.2 denominated as baseline).

This observation is often true for all the cavities treated with the standard doping method, instead, for the new thermal treatment proposed the situation can change dependently on the process parameters chosen. In fact it seems that, with the correct concentration gradient the maximum accelerating field increases, but intensive R&D is needed to understand how the doping affect negatively the quench field.

4.1 The low field Q-slope: a new possible explanation

The low field Q-slope (LFQS) is a peculiar feature generally found for cavities doped with impurities such as nitrogen [1]. Till now only two explanations were given to this phenomenon [14, 15]. The interpretation given in this section to the LFQS is an extension of the layer model [14], considering the variation of the BCS surface resistance with the mean free path.

Let us consider, in first approximation, a poor superconductive layer, of thickness a, with a London penetration depth λ_1, deposited on a second bulk good superconductor with a London

penetration depth λ_2. If an electromagnetic field with form $H_z(x) = H_z(0) \cdot e^{i(kx - \omega t)}$ is applied to the surface of such system, the field penetrates for a depth of the order of λ_1 inside the first superconductor. If $\lambda_1 > a$, then the field penetrates also in the second superconductor with a decay constant λ_2, as it is shown in Fig. 4.3.
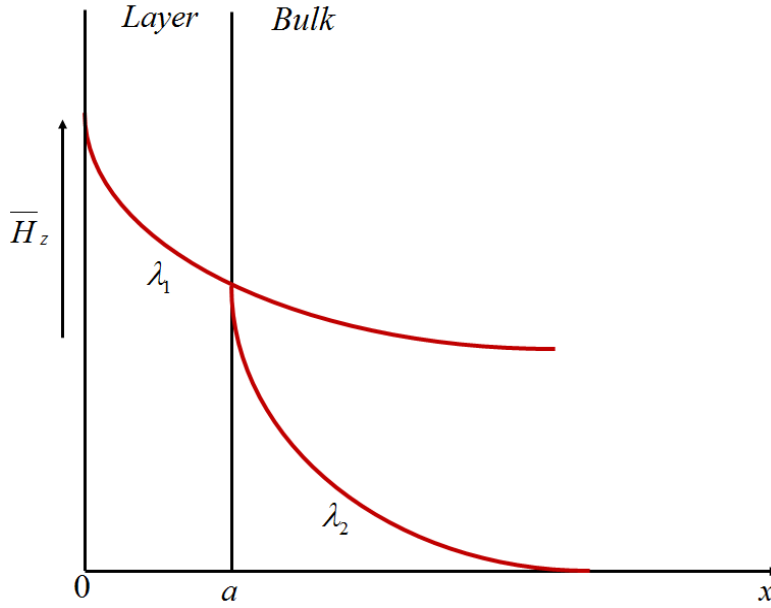
Figure 4.3: Schematic view of the magnetic field inside the superconductor layer - bulk superconductor system

The surface impedance of the system then will be:

$$Z = \frac{E_y(0)}{\int_0^\infty J_y(x)\, dx} = \frac{E_y(0)}{\int_0^a J_{y1}(x)\, dx + \int_0^\infty J_{y2}(x)\, dx} \tag{4.1}$$

where $J_{y1}(x)$ and $J_{y2}(x)$ are respectively the currents flowing in the first and in the second superconductor. Because the magnetic field can oscillates only in the thin layer defined by the London penetration depth, the two resulting currents have form:

$$J_{y1}(x) = J_0 \cdot e^{-\frac{x}{\lambda_1}}$$
$$\tag{4.2}$$
$$J_{y2}(x) = J_0 \cdot e^{-\frac{a}{\lambda_1}} \cdot e^{-\frac{x-a}{\lambda_2}}$$

where the following boundary condition was applied: $J_{y1}(a) = J_{y2}(a)$. By resolving the two integrals we obtain:

$$Z = \frac{E_y(0)}{J_0\lambda_1 \left(1 - e^{-\frac{a}{\lambda_1}}\right) + J_0\lambda_2 e^{-\frac{a}{\lambda_1}}} = \left[\frac{1}{Z_1}\left(1 - e^{-\frac{a}{\lambda_1}}\right) + \frac{1}{Z_2} e^{-\frac{a}{\lambda_1}}\right]^{-1} \tag{4.3}$$

Which means that the surface impedance is defined by two contributions summed in parallel but weighted over $\left(1 - e^{-\frac{a}{\lambda_1}}\right)$ and $e^{-\frac{a}{\lambda_1}}$. Where Z_1 and Z_2 are the surface impedances of the first and the second superconductors, respectively.

The reciprocal of equation Eq. 5.21 multiplied by the geometrical factor of the cavity g gives the value of the system Q-factor:

$$Q = Q_1 + \Delta Q \cdot e^{-\frac{a}{\lambda_1}} \tag{4.4}$$

where $\Delta Q = Q_2 - Q_1$ is the difference between the Q factors of the two superconductors.

Considering the first superconductor as a contaminated layer, its penetration depth should depend on the reduced magnetic field $b = B/B_c$ [14, 16], with B_c the critical magnetic field. We can then expand in series the penetration depth as follows:

$$\lambda_1(b) = \lambda_1(0) + \left.\frac{\partial \lambda_1}{\partial b}\right|_0 b + \cdots \cong \lambda_1(0) + \beta \cdot b \tag{4.5}$$

The situation now outlined implies a variation of the Q-factor with the field. As the field increases the penetration depth of the first layer also increases, therefore the bulk material becomes more and more important in defining the losses of the system. Because the layer is a poor superconductor, the bigger becomes its penetration depth the higher will be the contribute of the bulk material. A simulation of this Q-factor trend with the field is shown in Fig. 4.4.
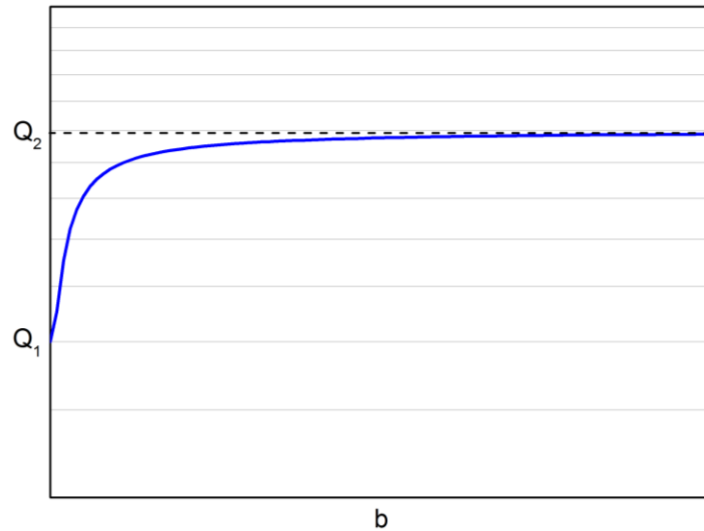
Figure 4.4: Q-factor versus reduced magnetic field simulation with the layer model.

The layer model, therefore, introduces a field dependence on Lambda which describes how the Q-factor may depends on field at lower accelerating gradients. By the way, it does not define a formulation on how determine the two superconductors' Q-factor.

In the case of a doped superconductor we should imagine a dopant concentration gradient from the surface to the material bulk. We can therefore suppose that, the mean free path, which is extremely dependent on the material purity, varies with the dopant concentration. Also, as it is derived in Appendix A, the BCS surface resistance has a dependence on the mean free path, with a minimum around $20 nm$. Hence, by combining these two assumptions comes out that the BCS surface resistance depends on the dopants concentration, and so, it varies with the dopants concentration profile in the material.

What should happen when the field is applied to such system is that, the London penetration depth increases as the field increases, therefore, the portion of material that the field is able to probe becomes bigger as the field gets bigger. This substantially means that, if a gradient of impurities is present, i.e. a gradient of R_{BCS}, then the value of Q_0 varies inversely respect the variation of R_{BCS} with the depth, how it is explained in the layer model, comporting the low field Q-slope effect.

The basic idea to modeling this situation in the simplest way is then to approximate the concentration gradient to a system composed of a layer of thickness a, with a certain mean free path l_1, deposited on a bulk superconductor with a mean free path l_2. Therefore, the two quality factors can be described by two different surface resistances, composed of a BCS part dependent on the mean free path and a constant residual resistance.

The R_{BCS} dependence on the mean free path is derived in Appendix A, here instead some algebra is done in order to express a simpler formulation for R_{BCS}. The BCS surface resistance implemented in this model is defined by the following formula (Eq. 4.6), already corrected by the multiplicative factor $1/2$ (Eq. 3.12) [10]:

$$R_{BCS} = \frac{1}{4}\left(\frac{\sigma_1}{\sigma_n}\right)\left(\frac{\omega\mu_0\alpha\rho_{ph}(300K)}{l}\right)^{\frac{1}{2}}\left(\frac{\omega\mu_0\lambda_L^2}{\alpha\rho_{ph}(300K)}l + \frac{1}{\frac{\sigma_2}{\sigma_n}}\right)^{\frac{3}{2}} \tag{4.6}$$

where:

$$\frac{\sigma_1}{\sigma_n} = \frac{2\Delta}{k_B T\left(1 + e^{-\Delta/k_B T}\right)^2}\ln\left(\frac{\Delta}{\hbar\omega}\right)e^{-\Delta/k_B T} \tag{4.7}$$

$$\frac{\sigma_2}{\sigma_n} = \frac{\pi\Delta}{\hbar\omega}\tanh\left(\frac{\Delta}{2k_B T}\right) \tag{4.8}$$

In the case under exam $T = 2K$, hence $T < T_c/2$ and some approximations can be done:

$$\left(1 + e^{-\Delta/k_B T}\right)^2 \cong 1$$

$$\tanh\left(\frac{\Delta}{2k_B T}\right) \cong 1$$

therefore, the Mattis and Bardeen integrals analytical solutions (Eq. 4.7, 4.8) become:

$$\frac{\sigma_1}{\sigma_n} \cong \frac{2\Delta}{k_B T} \ln\left(\frac{\Delta}{\hbar\omega}\right) e^{-\Delta/k_B T} \tag{4.9}$$

$$\frac{\sigma_2}{\sigma_n} \cong \frac{\pi\Delta}{\hbar\omega} \tag{4.10}$$

By some algebra it is possible to obtain the following formulation of Eq. 4.6:

$$R_{BCS} = \frac{1}{4}\left(\frac{\sigma_1}{\sigma_n}\right)\frac{\omega^2\mu_0^2\lambda_L^3}{\alpha\rho_{ph}(300K)}l\left(1 + \frac{\alpha\rho_{ph}(300K)}{\omega\mu_0\lambda_L^2 l\frac{\sigma_2}{\sigma_n}}\right)^{\frac{3}{2}} \tag{4.11}$$

And by direct substitution of Eq. 4.7 and $\alpha = \frac{\omega\mu_0\xi_0\lambda_L^2}{\rho_{ph}(300K)}\frac{\sigma_2}{\sigma_n} \cong 27\text{Å}$, we obtain:

$$R_{BCS} = \frac{1}{2}\frac{\Delta}{k_B T}\ln\left(\frac{\Delta}{\hbar\omega}\right)\frac{\omega^2\mu_0^2\lambda_L^3}{\alpha\rho_{ph}(300K)}l\left(1 + \frac{\xi_0}{l}\right)^{\frac{3}{2}} \cdot e^{-\Delta/k_B T} \tag{4.12}$$

Therefore, the BCS surface resistances of the two superconductors can be defined as:

$$R_{BCS1} = C \cdot l_1\left(1 + \frac{\xi_0}{l_1}\right)^{\frac{3}{2}} \cdot e^{-\Delta/k_B T} \tag{4.13}$$

$$R_{BCS2} = C \cdot l_2\left(1 + \frac{\xi_0}{l_2}\right)^{\frac{3}{2}} \cdot e^{-\Delta/k_B T} \tag{4.14}$$

where:

$$C = \frac{1}{2}\frac{\Delta}{k_B T}\ln\left(\frac{\Delta}{\hbar\omega}\right)\frac{\omega^2\mu_0^2\lambda_L^3}{\alpha\rho_{ph}(300K)} \tag{4.15}$$

Using Eq. 4.13 and 4.14 we can then define the layer model extended to the case of a doped superconductor, as follows:

$$Q(b) = \frac{g}{R_{BCS1} + R_{res}} + \left(\frac{g}{R_{BCS2} + R_{res}} - \frac{g}{R_{BCS1} + R_{res}} \right) \cdot e^{-\frac{a}{\lambda_1(0) + \beta \cdot b}} \qquad (4.16)$$

Where $g = 270\Omega$ is the geometrical factor for the $1.3GHz$ TESLA type elliptical cavities studied at FNAL, and R_{res} the residual resistance, which is considered constant for the two superconductors.
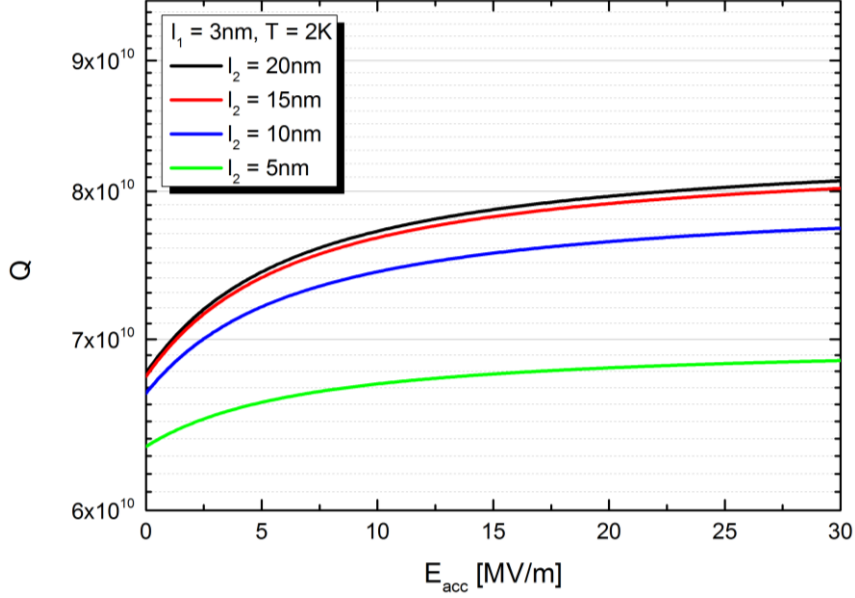
Figure 4.5: Some simulation of the Q-factor's trend with the accelerating field for two superconductor with different mean free path.

In order to express the dependence of the Q-factor respect to the accelerating gradient E_{acc}, instead of the reduced magnetic field b, we can write:

$$B[mT] = \varepsilon \cdot E_{acc}[MV/m] \qquad (4.17)$$

where $\varepsilon = 4.25MV \cdot mT^{-1}m^{-1}$ is the conversion factor between the magnetic field expressed in mT and the accelerating field expressed in MV/m. In Fig. 4.6 it is shown a simulation of the LFQS using Eq. 4.16 and the following parameters:

Coherence length, ξ_0	$23 \cdot 10^{-9}m$
London's penetration depth, λ_L	$40 \cdot 10^{-9}m$
Critical temperature, T_c	$9.23K$
Critical field, H_0	$2000G$
Phonon resistivity at $300K$, $\rho_{ph}(300K)$	$1.45 \cdot 10^{-7}\Omega \cdot m$

Frequency, f	$1.3 \cdot 10^9 Hz$
Temperature, T	$2K$
Dirty layer's mean free path, l_1	$3 \cdot 10^{-9} m$
Residual resistance, R_{res}	$1 \cdot 10^{-9} \Omega$
Lambda expansion constant, β	$1 \cdot 10^{-6} m$
Layer thickness, a	$1 \cdot 10^{-7} m$

How it can be seen, the simulation gives a trend of the Q-factor with the accelerating field very close to the experimental data. In order to corroborate the model also some fits on the experimental data were done.

This model is by the way not complete, but only an approximation. Indeed, the model was implemented by thinking about a dirty superconductive layer deposited on a clean bulk superconductor. This is actually a roughly approximation, because a continuous variation of impurities is present. Therefore, the correct description would be the subsection of infinitesimal layers with different purity, i.e. different mean free path and penetration depth. In this situation, as suggested in [14], the shape of the Q-factor curve should be described by:

$$\lim_{n \to \infty, a \to 0} Q = \int_0^\infty \frac{dQ(x)}{dx} e^{-\int_0^\infty \frac{1}{\lambda(\bar{x})} d\bar{x}} dx \tag{4.18}$$

The future idea is then to implement this more correct formulation in the model.

4.1.1 Experimental data fit

In order to interpolate the experimental data with such Section 6.

The dependence of the critical magnetic field and of the superconductive energy gap on the temperature were taken into account with:

$$H_c(T) = H_0 \left[1 - \left(\frac{T}{T_c} \right)^2 \right] \tag{4.19}$$

$$\Delta(T) = 1.76 k_B T_c \left[\cos \left(\frac{\pi}{2} \left(\frac{T}{T_c} \right)^2 \right) \right]^{1/2} \tag{4.20}$$

The values of R_{BCS1} and R_{BCS2} were instead calculated with Eq. 4.13 and 4.14. Because of the high degree of dependence between the parameters, it is was chosen to leave free only three parameters. In order to define the Q-factors of the dirty layer and of the bulk superconductors, and the shape and the elongation of the LFQS, the two respective mean free paths (l_1 and l_2) and the layer thickness a were left as free parameters. Whereas, the penetration depth expansion constant β was fixed to a specific value, which was adjusted case by case. Obviously, the fit was performed once the initials parameters were chosen in proper way, in order to be sure that the fit converged.

The fit parameters initialization was done by acting on the values of the layer thickness a, and on the penetration depth expansion constant β. In Fig. 4.7 it is shown how these two parameters modify the quality factor curve shape. These curves were calculated with the following values of mean free path: $l_1 = 1nm, l_2 = 5nm$.
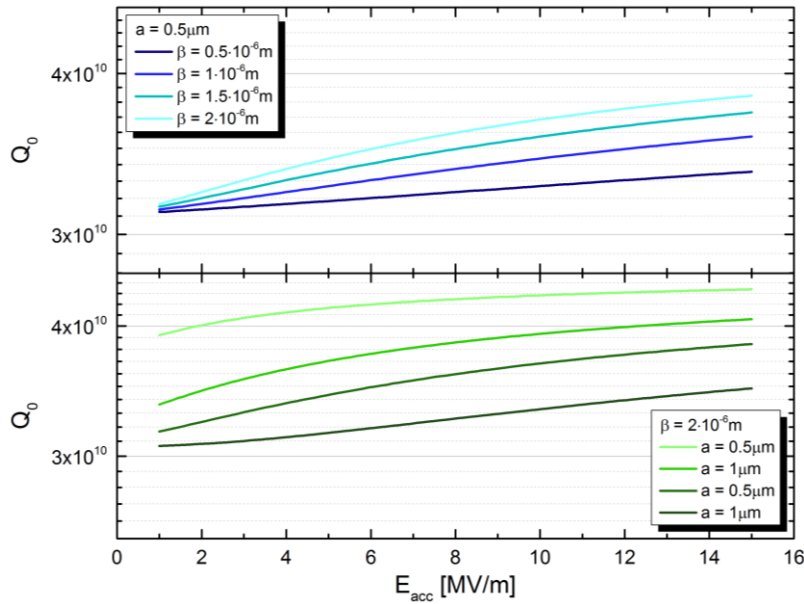
Figure 4.6: Simulation of the LFQS-fit function with different value of β and a.

As β increases, the elongation of the low field Q-slope decreases, and the curve slope will be higher. This because as β gets bigger, the exponential weighting factor $e^{-\frac{a}{\lambda_1(0)+\beta \cdot b}}$ in Eq. 4.16 tends to 1, therefore the contribution of the bulk material appears strongly also at very low fields.

On the other hand, if the dirty layer thickness a gets lower, then the field inside the London penetration depth probes more bulk material, even at lower fields, therefore because of the lower overall surface resistance the Q-factor is enhanced, the curves is shifted to high values and the slope of the LFQS becomes slightly higher. In practice, the variation of β and a gives the same results, but in orthogonal way.

The choice of these two parameters is really tricky, and in order to obtain a good fit it is mandatory to fix at least one of them. It was chosen to fix β instead of a, because the first one, how it can be seen in Eq. 4.5, is the first order expansion constant of the London penetration depth of the first layer. Hence, if β was left free the determination of l_1, and subsequently λ_1, would depend on it. Therefore, there would be mutual decency between these two parameters and the fit would not converge.

By the way, once the initializing parameters were found, the fit was iterated leaving free both the mean free paths of the dirty layer and the bulk and the dirty layer thickness. The other parameters of the fit were instead fixed, as it is shown in the following list:

Coherence length, ξ_0	$40 \cdot 10^{-9} m$
London's penetration depth, λ_L	$23 \cdot 10^{-9} m$
Critical temperature, T_c	$9.23 K$
Critical field, H_0	$2000 G$
Phonon resistivity at $300K$, $\rho_{ph}(300K)$	$1.45 \cdot 10^{-7} \Omega \cdot m$
Frequency, f	$1.3 \cdot 10^9 Hz$
Temperature, T	$2K$
RRR - mean free path conversion, α	$27 \cdot 10^{-10} m$
Geometrical factor, g	270Ω

The residual resistance was set to a suitable value case by case, trying to maintain it around $3n\Omega$, which can be consider a pretty good mean of the residual resistance values found in the literature [1]. By the way, this value is really ponderous in the determination of the Q-factor, because it comports the shift of the curve to higher or lower values, by leaving the other parameters practically unchanged.

In Fig. 4.8 it is shown a fit on the data of the cavity TE1AES013.
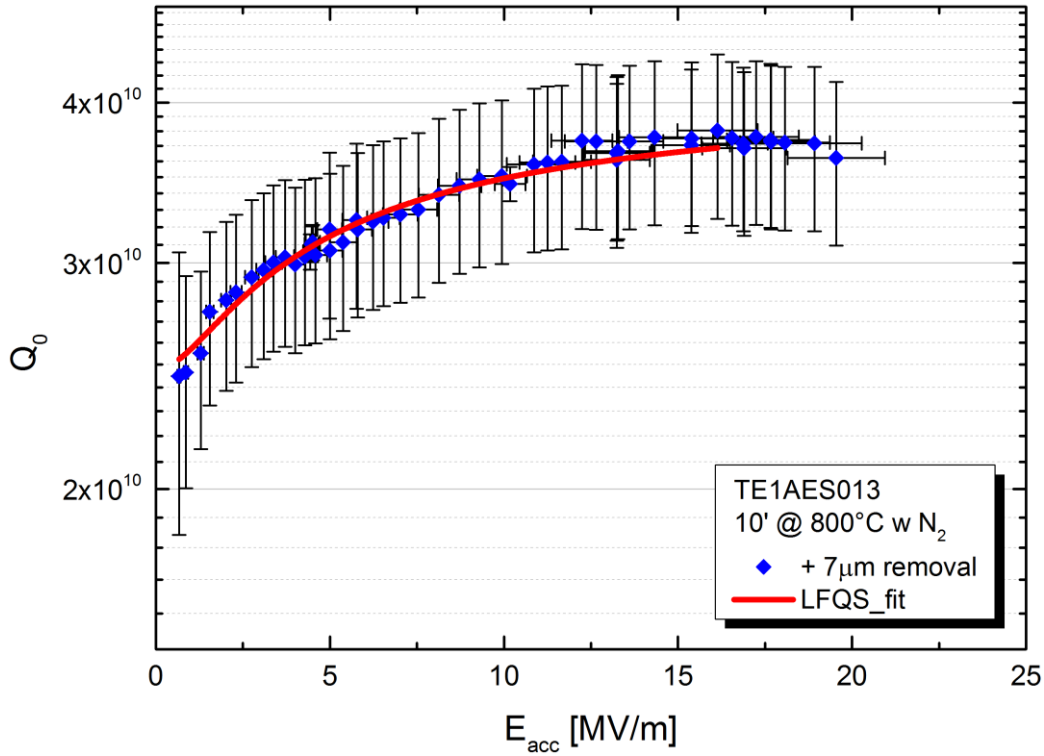
Figure 4.7: LFQS fit on cavity TE1AES013 after thermal doping and $7\mu m$ of material removal.

The fixed parameters and the fit results are shown in the following table (Tab. 4.2).

Parameter	Value	Standard Error	Status
R_{res}	$3.3{\cdot}10^{-9}\,\Omega$	0	Fixed
l_1	$4.2{\cdot}10^{-10}$ m	$0.9{\cdot}10^{-10}$ m	Free
l_2	$4.5{\cdot}10^{-9}$ m	$0.3{\cdot}10^{-9}$ m	Free
a	$6.1{\cdot}10^{-7}$ m	$0.8{\cdot}10^{-7}$ m	Free
β	$5{\cdot}10^{-6}$	0	Fixed
λ_1	$2.2{\cdot}10^{-7}$ m	$9.4{\cdot}10^{-16}$ m	Calculated
λ_2	$7.3{\cdot}10^{-8}$ m	$3.2{\cdot}10^{-15}$ m	Calculated

Table 4.2: Fit parameters for cavity TE1AES013.

What comes out from the fit results is that actually in correspondence of the maximum of the Q_0 versus E_{acc} curve the mean free path does not correspond to the minimum of the BCS surface resistance, which instead presents the minimum in correspondence of $\sim 20nm$. Indeed, the mean free path at the maximum of the Q-factor curve calculated from the fit is equal to $l_2 = 4.52(0.3)\ nm$, which correspond to a superficial London's penetration depth of $73nm$. On the other hand, the dirty layer's mean free path is $l_1 = 0.42(0.09)\ nm$, therefore Niobium at the surface is completely in the dirty limit and the penetration depth is in fact equal to $220nm \gg \xi_0$.

The same fit was done to cavity TE1AES011, which was treated with the new approach to the cavity doping with the high temperature process proposed. The fit is shown in Fig. 4.9, while the fit parameters are listed in the following table (Tab. 4.3).
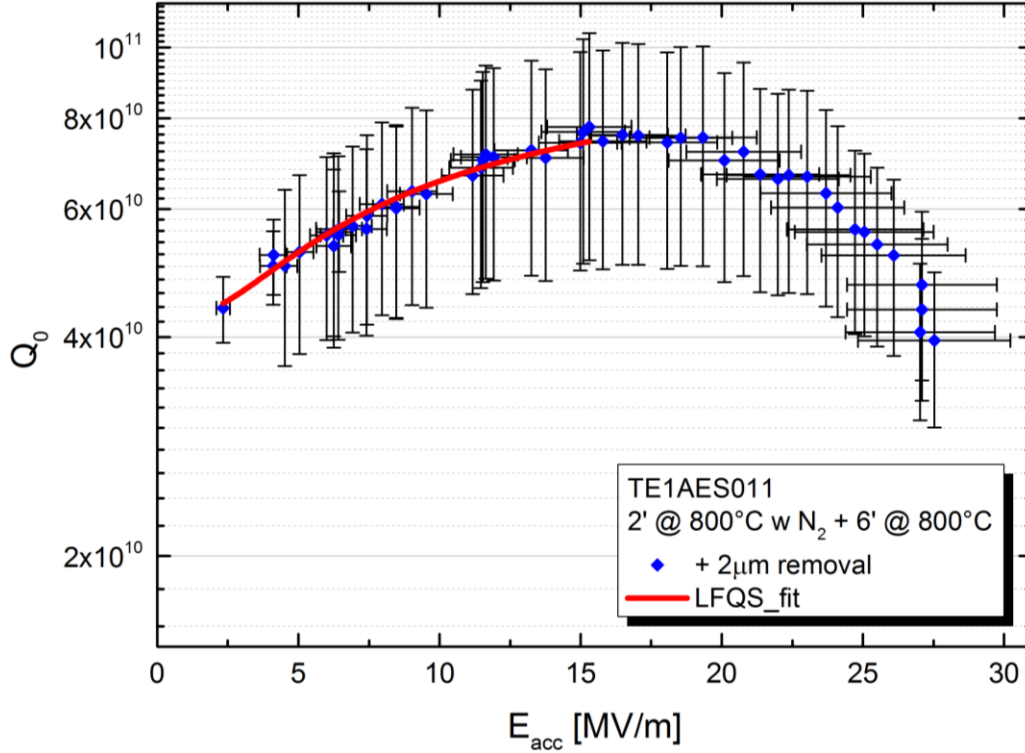
Figure 4.8: LFQS fit on cavity TE1AES011 after the new thermal doping approach.

Parameter	Value	Standard Error	Status
R_{res}	$0.3 \cdot 10^{-9}\,\Omega$	0	Fixed
l_1	$8.3 \cdot 10^{-10}$ m	$0.6 \cdot 10^{-10}$ m	Free
l_2	$1.4 \cdot 10^{-8}$ m	$0.7 \cdot 10^{-8}$ m	Free
a	$1.2 \cdot 10^{-6}$ m	$0.1 \cdot 10^{-6}$ m	Free
β	$5.4 \cdot 10^{-6}$ m	0	Fixed
λ_1	$1.6 \cdot 10^{-7}$ m	$6.4 \cdot 10^{-16}$ m	Calculated
λ_2	$4.5 \cdot 10^{-8}$ m	$7.3 \cdot 10^{-14}$ m	Calculated

Table 4.3: Fit parameters for cavity TE1AES011.

From the parameters calculated it comes out that the mean free path, in correspondence of the maximum of the curve Q_0 versus E_{acc} ($l_2 = 14(7)nm$, $\lambda_2 = 45nm$), quite corresponds to the minimum value of the BCS surface resistance. The value associated to the mean free path of the dirty layer is found to be $0.83(0.06)nm$, therefore this is anyhow in the London dirty limit ($\lambda_1 = 160nm \gg \xi_0$), but a little bit cleaner than cavity TE1ASE013.

Anyhow, it is necessary to remember that this cavity was measured in over coupling condition, therefore the experimental data of unloaded Q-factor are affected by a systematic error, which shifts the whole curve to higher values.

This fact substantially explains why the value of the residual resistance used is so low, and it is not close to the literature mean value of $3n\Omega$. By decreasing this value it was possible to fit the curve, which otherwise would not be interpolated. Therefore, we expect that the real value of residual resistance would be higher and comparable with the literature, instead the values of the two mean free paths would be more or less correct. This because, if the cavity was measured in critical coupling, then curve would be at lower values, and by fixing a higher value of residual resistance, the fit would probably converged anyway without modifying so much the mean free paths values.

In the two fits done the data points after the Q-factor maximum were masked. This because, the fit function implemented cannot interpolate the values for fields bigger than the value at which the maximum Q value falls. Indeed, the layer model, from which this model is defined, was thought to interpolate only the LFQS, and not the medium field or high field Q-slopes. Anyhow, the pronounced high field Q-slope just after the maximum of Q-factor in cavity TE1AES011, is certainly due to some other kinds of dissipations which in this thesis are not discussed.

It is important to underline that, the mean free path calculated from the fit is only a way to define the London penetration depth of the first and the second layer in a more convenient way. Therefore, when a very low mean free paths are obtained this substantially means larger London penetration depths:

$$\lambda = \lambda_L \left(1 + \frac{\xi_0}{l} \right)$$

but if the value of the London penetration depth at the surface was also dependent on other contributions, besides the mean free path, the value of the mean free path estimated from the fit would be wrong, and probably underestimated, if λ was too big. Therefore, my personal opinion is that something happens just below the surface of the superconductor which we still do not understand. For example, if we consider the discoveries reported in [5, 17] it comes out that exists some deviation from the ideal Meissner effect described by the second London equation. In fact, just below the surface, a "dead layer" of several nanometers is present, within the magnetic field is more or less constant and with the same value of the applied field. This suggests that, in the first nanometers inside the material the London penetration depth is actually different from the bulk, and this may comport the underestimation of the mean free path at the surface calculated by the model. Hence, even though the model returns superficial mean free paths lower than the literature ones, to what concern Niobium [13], the information obtained from the fit are anyhow

reliable. This because, they can give us qualitative information about the dopants concentration, and distribution, in the material.

In order to understand what this model can suggest us about the dopants concentration profile in the material, we have to think about the values of the layer thickness a and the value of the constant β obtained. If a large β value is obtained, this substantially means that as the field increases the Q-factor increases quickly, because the field inside $\lambda_1(E)$ can probe more deeper material, which is supposed to have lower resistance. Therefore, the slope of the Q-factor should be higher.

The same effect is observed if a has low values. In this situation the dirty layer - bulk interface is near the surface, so the field inside $\lambda_1(E)$ can reach it even at low field values, implying a LFQS more sloped.

If we merge together these last assumptions with the concentration profile in the material, it comes out that if β is big, then the field probes deeper zones of the material even at low field. Hence, we aspect that the correct concentration would not be at the surface, but probably deeper inside the material. If instead a little β is obtained, the field is not able to probe the deeper material for low values of accelerating field, therefore the slope of the curve appears lower and the correct concentration should be near the surface.

On the other hand, if a is little the concentration profile is supposed to have a certain gradient, which increases as a decreases, and with a not corrected concentration at the surface. This because if the layer - bulk interface is near the surface, then the penetration depth can feel the underlying bulk superconductor contribution, even at low field. Hence, the Q-factor increases rapidly with the accelerating gradient. Instead, if a is big this means that the concentration profile is probably more flat, and the variation of the quality factor with the field is less rapid.

In order to explain this effect, let us consider the dopants concentration profiles expected for the two cavities studied (Fig. 4.10) after the thermal treatment and chemistry. If we take into account cavity TE1AES013, it can be seen that, the thickness of the dirty layer is lower than cavity TE1AES011 (Tab. 4.2, 4.3), therefore the cavity TE1AES013 correct concentration is closer to the surface than the other cavity. This, as mentioned before, suggests a more pronounced impurities gradient.

On the other hand, dirty layer thickness of the cavity TE1AES011 is practically double than the one of TE1AES013, this means that the correct concentration is more deep inside the material, so the concentration gradient is supposed to be more flat. The values of β are instead almost the same, for cavity TE1AES011 is slightly higher and this is in accordance with the dopants concentration gradient inside the material. Concluding, the value of a is higher for cavity TE1AES011 than for cavity TE1AES013, and also the values of β. Therefore, the actual

concentration gradient is more flat for cavity TE1AES011, indeed, the accelerating field at which the Q-factor has a maximum is higher and the LFQS is more elongated.
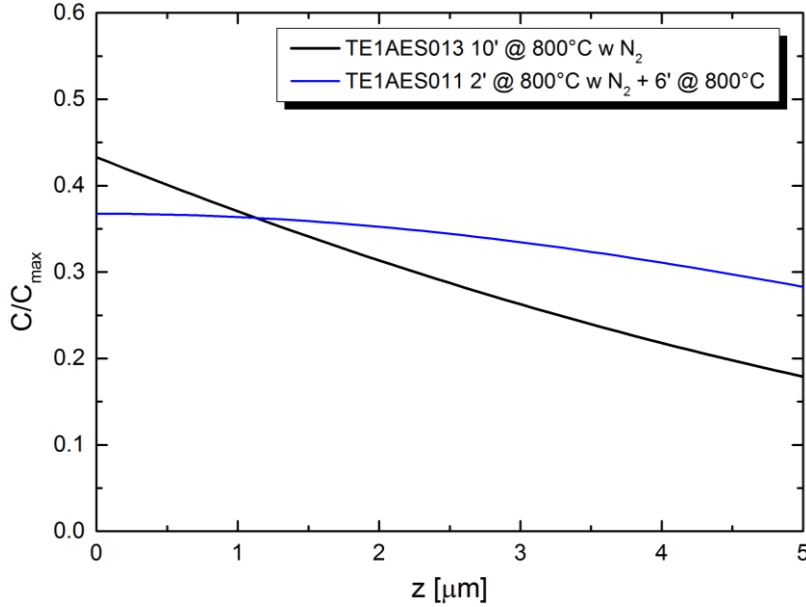
Figure 4.9: Dopants diffusion profiles expected after the thermal treatment and the subsequent chemistry.

Therefore the idea is that, by preparing cavities with flat concentration profiles, and with the correct concentration right from the surface, probably the Q-factor curve versus the accelerating field will be flatter and at higher values.

Anyhow, this model gives only a roughly explanation of the LFQS, the variation of the surface resistance as a simple variation of the mean free path is of course an approximation. The presence of a diffusion profile of impurities may imply other not negligible effects. A more complete model should take into account also the variation of the lattice constant, which widely affects the superconducting behavior of the material. For example, the strong coupling parameter s is very sensitive to the lattice condition, and it affects directly the superconductive energy gap, indeed:

$$\Delta_0 = \frac{s}{2} k_B T_c$$

Therefore, if s increases also Δ_0 increases, leading to a decreasing of the BCS surface resistance, implying higher quality factors.

Another effect that can play inside the superconductive energy gap, which depends on the lattice conditions, is the critical temperature dependence on the interaction between electrons and phonons described by the phenomenological Mc Millan formula:

$$T_c = 1.14\Theta_D e^{-\left(\frac{1}{\lambda-\mu^*}\right)}$$

where λ is the electron-phonon interaction, μ^* is the electron-electron repulsive interaction and Θ_D the Debye temperature.

The presence of impurities might modify the strength of the electron-phonons interactions, and from my point of view light atoms, like Nitrogen, should be able to oscillate more than Niobium atoms, hence the electrons screening should be enhanced. This implies directly, that the Cooper pairs formation is favored and therefore an increment of T_c is expected. An increasing of T_c is then directly connected to the increasing of the superconductive energy gap, hence to a decrement of the BCS surface resistance.

What comes out from these assumptions is that probably the real explanation of the LFQS, obtained through the cavity doping, is due to a combination of several effects, which depend closely to the lattice condition and to the purity of the material. By the way, the main limitation of such model is intrinsic of the layer model from which is derived. The correct dependence of the penetration depth respect to the field should be described considering a continuous of infinitesimal layers, each one with its mean free path and penetration depth. As discussed previously, Eq. 4.18 may be used in order to take into account the real distribution of impurities in the material.

5 Conclusions

The results obtained, are surprising, indeed, even though the first cavity shows low Q-factor and low quench field, the other one, shows higher quality factor and higher quench field than the cavities treated with the classical doping method. Also, the fingerprint of Nitrogen-doped cavities, i.e. the low field Q-slope (LFQS), in the first cavity it is negligible, while in the second one it is really pronounced. The two cavities, indeed, were appositely prepared in order to obtain two different concentration profiles. Therefore, the first conclusion we can done is that the LFQS is actually function of the concentration profile.

In order to corroborate this idea, it was implemented a model to describe the LFQS as a direct consequence of the concentration profile of dopants inside the material. What was underlined by such model is that, the increasing of the quality factor with the field is due to the BCS surface resistance variation with the impurity content, i.e. the mean free path. While the shape of the curve is affected from the shape of the diffusion profile. Indeed, the model suggests that flatter concentration profiles should return more elongated LFQS, while high gradients of impurity should return more sloped LFQS with lower elongation.

By the way, such model approximate the diffusion profile into a system composed of a superconductive layer deposited on a bulk superconductor, therefore the results are only an estimation, and give only qualitative information. Hence, the next step will be the extension of this model to a continuous of infinitesimal layers with different mean free path, in order to be able to perform the simulation of the concentration profile, directly from the quality factor versus accelerating field curve of the cavity.

6 The Low Field Q-slope Fit Code

Is here reported the fit code developed with the data analysis program OriginPro9®, to interpolate the low field Q-slope found for the cavities doped with Nitrogen:

```
void _nlsfAntiQSlopeApprox(

// Fit Parameters:

double LamL, double Xi0, double g, double f, double Tc, double
T, double l1, double l2,double beta, double a, double Rres,
double z, double alpha,

// Independent Variables:

double x,

// Dependent Variables:

double& y)

{

    const double K=8.6177*10^(-5); //Const. Boltzmann

    const double h=4.136*10^(-15); //Const. Plank

    const double mu0=1.25665*10^(-6); //Magn. permittivity

    const double Rph=1.45*10^(-7); //Phonon resistivity

    const double H0=2000; //Critical field @ T = 0K

    double c = (mu0^2*(2*pi*f)^2)/(alpha*Rph); //Constants

    double Delta = 1.76*K*Tc*sqrt(cos(pi/2*(T/Tc)^2));  //Delta
                                              temperature
                                              dependence
```

```
double Hc = H0*(1-(T/Tc)^2); //Critical field temperature
                                dependence

double    S1    =    ((Delta/(K*T)))*ln(Delta/(h*f))*exp(-
Delta/(K*T)); //Numerical solution M-B first integral

double B = 4.25*x*10^(-3)*10^(4); //Electric field
                                conversion [MV/m - G]

double Lam1 = LamL*(1+(Xi0/l1))^(1/2); //London penetration
                                layer

double Lam2 = LamL*(1+(Xi0/l2))^(1/2); //London penetration
                                bulk

double LamE = Lam1+((beta*B)/Hc); //Field dependent London
                                penetration depth

double R1 = z*c*S1*l1*Lam1^3 + Rres; //Rs layer

double Q1 = g/R1; //Q layer

double R2 = z*c*S1*l2*Lam2^3 + Rres; //Rs bulk

double Q2 = g/R2; //Q bulk

y = Q1+(Q2-Q1)*exp(-a/LamE) //LFQS_fit
}
```

The fit parameters where initialized case by case, by the way the starting parameters where:

Coherence length, Xi0	$40 \cdot 10^{-9} m$	Fixed
London's penetration depth, LamL	$23 \cdot 10^{-9} m$	Fixed
Geometrical factor, g	270Ω	Fixed
Critical temperature, Tc	$9.23 K$	Fixed
Frequency, f	$1.3 \cdot 10^9 Hz$	Fixed
Temperature, T	$2 K$	Fixed

Residual resistance, `Rres`	$3 \cdot 10^{-9}\Omega$	Fixed
Lambda expansion constant, `beta`	$5 \cdot 10^{-6}m$	Fixed
R_{BCS} correction factor, `z`	0.5	Fixed
RRR - mean free path conversion, `alpha`	$27 \cdot 10^{-10}m$	Fixed
Dirty layer's mean free path, `l1`	$1 \cdot 10^{-9}m$	Free
Bulk's mean free path, `l2`	$5 \cdot 10^{-9}m$	Free
Layer thickness, `a`	$5 \cdot 10^{-7}m$	Free

References

[1] Grassellino et al. *Supercond. Sci. Technol.* **26**, 102001 (2013)

[2] H. Mehrer *Diffusion in Solids*, Springer Series in Solid-State Sciences (2007)

[3] R. W. Powers, M. V. Doyle, *J. Appl. Phys.* **30**, 514 (1959)

[4] Grassellino et al. arXiv:1305.2182

[5] Romanenko et al. - arXiv:1311.7153

[6] A. Abrikosov *Fundamentals of the Theory of Metals*, North-Holland (1988)

[7] S. B. Nam *Phys. Rev.* **156**, 470 (1967)

[8] S. B. Nam *Phys. Rev.* **156**, 487 (1967)

[9] D. C. Mattis, J. Bardeen *Phys. Rev.* **111**, 412 (1958)

[10] V. Palmieri *Tutorials of the 16th International Conference on RF Superconductivity*, Paris 2013

[11] H. Padamsee *RF Superconductivity - Science, Technology and Applications*, Wiley-VHC (2009)

[12] B. Pippard *Proc. R. Soc. Lond. A* **216**, 547 (1953)

[13] K. Saito, P.Kneisel *Proceedings of the 9th Workshop on RF Superconductivity* **TUP031**, Santa Fe 1999

[14] V. Palmieri *Proceedings of the 12th International Workshop on RF Superconductivity* **TUA02**, Cornell University, Ithaca 2005

[15] Xiao, C. E. Reece *Proceedings of the 16th International Conference on RF Superconductivity* **MOIOC02**, Paris 2013 **(on press)**

[16] V. Palmieri private talks

[17] Suter et al. *Phys. Rev. B* **72**, 024506 (2005)